



Open Access: ISSN 1847-9286

www.jESE-online.org

Original scientific paper

Evaluation of the electrochemical performance of Ag containing AAO layers after extended exposure to a model corrosive medium

Stephan Kozhukharov^{1,✉}, Christian Girginov², Denitsa Kiradzhiyska³, Aleksander Tsanev⁴ and Georgy Avdeev⁵

¹LAMAR Laboratory for Advanced Materials Research, University of Chemical Technology and Metallurgy, Sofia, Bulgaria

²Department of Physical Chemistry, University of Chemical Technology and Metallurgy, Sofia, Bulgaria

³Medical University Plovdiv, Department of Chemical Sciences, Faculty of Pharmacy, Plovdiv, Bulgaria

⁴Institute of General and Inorganic Chemistry, Bulgarian Academy of Sciences, Sofia, Bulgaria

⁵Institute of Physical Chemistry, Laboratory of X-Ray Diffraction Methods, Bulgarian Academy of Sciences, Sofia, Bulgaria

Corresponding author: ✉ stephko1980@abv.bg; Tel.: +35 9899837282

Received: March 25, 2020; Revised: May 30, 2020; Accepted: May 31, 2020

Abstract

The coating procedure appears to be an indispensable finishing stage in the production of Al based industrial products, engineering facilities and equipment. For this reason, there is an ever-increasing interest towards the elaboration of reliable corrosion protective layers with apparent coverage, adhesion, and barrier properties. In this sense, both the formation of anodized aluminum oxide (AAO) layer and its further modification with silver enable the elaboration of advanced (Al-O-Ag) films with extended beneficial characteristics. The present research activities are aimed at the determination of the corrosion protective properties of electrochemically synthesized Al-O-Ag layers on the technically pure AA1050 alloy. The structures and compositions of the obtained Al-O-Ag layers were characterized by X-ray diffractometry (XRD) and X-ray photoelectron spectroscopy (XPS). The research activities were accomplished by means of two independent electrochemical characterization methods: electrochemical impedance spectroscopy (EIS) and potentiodynamic scanning (PDS). The electrochemical measurements were performed after 24, 168 and 672 hours of exposure to 3.5 % NaCl solution used as a model corrosive medium (MCM), in order to determine the barrier properties and durability of the elaborated Al-O-Ag layers. The analysis of the obtained results has undoubtedly shown that the proposed electrochemical Al-O-Ag layer formation can successfully be used for the creation of self-standing layers with apparent corrosion protective properties. Besides, Al-O-Ag system can be used as a basis for

development of efficient protective layers suitable for application in biologically contaminated media.

Keywords

Al-O-Ag layers, porous structures, compositions, protective abilities.

Introduction

The widest field of use of the low doped Al alloys, such as AA1050 is the packaging of various nutrition products and soft drinks [1-4]. However, reliable packaging requires additional surface protection of Al-based materials, prior to being in contact with whatever nutrition product. This requirement arises for prevention of Al-ions resorption from such packaging materials [5-7], which endangers human health [8,9]. Anodization is a simple and reliable method for the formation of highly-ordered and self-organized porous oxides [10-14]. This method enables the formation of reliable, large-scale, protective oxide layers using relatively simple equipment. Besides, the resulting anodized aluminum oxide (AAO) possesses remarkable corrosion protective abilities after extended periods of exposure to model corrosive media [15,16].

The incorporation of silver is an efficient method for the further extension of the corrosion protective properties of the already formed AAO layers because Ag-compounds prevent the occurrence of *Microbially Influenced Corrosion* (MIC). MIC is an electrochemical process where micro-organisms can initiate, facilitate or accelerate corrosion reactions through interaction among the components of the metal-solution-microorganisms system [17]. According to recent research, MIC can appear in various media [18,19], including water supply and irrigation pipe systems [19], marine environments [20], in both tropic [20] and arctic [21] conditions, also in fuel tanks [22,23], etc. Figure 1 presents a schematic illustration of localized MIC on aluminum alloy, according to the concepts described in [14].

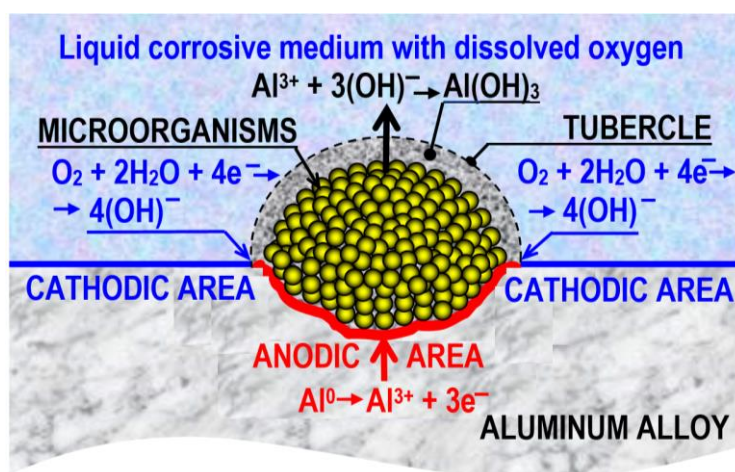


Figure 1. Schematic presentation of microbial tubercle causing localized MIC according [14]

The beneficial properties of silver and its ions are not limited only to their confirmed bactericide properties, recently widely investigated [24–40]. Materials, containing this element possess also definitively catalytic [41–43] and photocatalytic [44–57] properties. Furthermore, Bu *et al.* [58] have proposed even hydrogen production by Ag_2O based photocatalyst.

The specific combination of the benefits provided by anodization and the further deposition of silver applied to the widely used low-doped aluminum alloy has inspired the present research on the surface characteristics and corrosion protective abilities of the resulting Al-O-Ag films in comparison to unmodified AAO layers and bare Al samples. In this sense, the present study is an

extension of previous systematic research works [59,60] devoted to such electrochemically synthesized Al-O-Ag layers.

The aim of the present paper is to clarify the structural and compositional features of the electrochemically synthesized Al-O-Ag films on the conventional AA1050 alloy and to define their corrosion protective capabilities up to 672 hours of exposure to 3.5 % NaCl solution (serving as MCM). The clarification of these aspects should further extend the investigations already performed on the proposed electrochemically synthesized Al-O-Ag layer.

Experimental

Surface treatments and films formation

All experimental procedures were performed on three sets of samples, represented by two Al AA1050 coupons. The metallic samples underwent the surface treatment procedures, described in Table 1.

Table 1. Description of samples and film preparation conditions

Sample groups	Surface treatment procedures		
References	Preliminary treatments	-	-
AAO layers	Preliminary treatments	Anodization	-
Al-O-Ag layers	Preliminary treatments	Anodization	Silver deposition

Preliminary treatment: This step included annealing, degreasing in CCl_4 and final washing with double-distilled water, followed by brightening in solution, containing CrO_3 (20 g dm^{-3}) and 85 % H_3PO_4 ($15 \text{ cm}^3 \text{ dm}^{-3}$), at $85 \text{ }^\circ\text{C}$. These procedures were finished by further cleaning with tap and double-distilled water and subsequent drying at room temperature.

Anodization: This process was performed in 15 wt% H_2SO_4 at constant current density ($15 \times 10^{-3} \text{ A cm}^{-2}$) at $20 \text{ }^\circ\text{C}$, for 50 min. Two of these samples were set apart and denominated as AAO layers. Finally, all anodized specimens were washed with tap and double-distilled water and dried at room temperature.

Silver deposition: This final stage was carried out by AC-polarization (sinusoidal, 50 Hz) at a nominal voltage of 20 V in an electrolyte, composed of AgNO_3 (1.51 g dm^{-3}) and H_3BO_3 (45 g dm^{-3}), at $20 \text{ }^\circ\text{C}$. The resulting specimens were designated as Al-O-Ag film samples. Finally, these samples were also cleaned and dried under the above-mentioned conditions.

Comparative test procedures

The already treated samples underwent surface analyses by means of *X-ray diffractometry* (XRD), *X-ray photoelectron spectroscopy* (XPS) and also electrochemical analyses after extended periods of exposure to chloride containing MCM.

X-ray diffractometry: This analysis was performed with a Philips PW 1050 vertical automatic diffractometer, equipped with a secondary graphite monochromator, operating with $\text{CuK}\alpha$ radiation and scintillation counter. The diffraction curves were recorded in angular interval from 10 to 80 angular degrees 2θ with step 0.04° and 1 sec exposure.

XPS analysis: XPS measurements were carried out on preliminary scraped Al-O-Ag layer by AXIS Supra electron-spectrometer (Kratos Analytical Ltd.) using achromatic $\text{AlK}\alpha$ radiation with a photon energy of 1486.6 eV. Aiming for more detailed spectra, the emission current for the spectra of Ag3d and Ag MNN was set to 25 mA and the resolution was 40, while for the wide scan the emission current was 15 mA and the resolution was 160. The energy calibration was performed by

normalizing the C1s line of adsorbed adventitious hydrocarbons to 284.6 eV. The *binding energies* (BE) were determined with an accuracy of ± 0.1 eV. The changes in composition and chemical surrounding in the depth of the films were determined monitoring the areas and binding energies of C1s, O1s, Ag3d and Al2p photoelectron peaks. Using the commercial data-processing software of Kratos Analytical Ltd. the concentrations of the different chemical elements (in atomic %) were calculated by normalizing the areas of the photoelectron peaks to their relative sensitivity factors.

Electrochemical analysis: These measurements were performed employing two analytical electrochemical methods, after 24, 168 and 672 hours of exposure to 3.5 % NaCl solution as *model corrosive medium* (MCM). These electrochemical techniques were *electrochemical impedance spectroscopy* (EIS) and *potentiodynamic scanning* (PDS). The EIS spectra acquisitions were performed using a three-electrode configuration connected to Autolab PG-stat 30, equipped with a frequency response analyzer (FRA-2 module). The electrochemical cells containing 100 ml of MCM, provided radial concentric positioning of the electrodes. All measurements were performed against an Ag/AgCl/3M KCl reference electrode positioned 10 mm above the *corrosion test areas* (CTA) of the specimens. The electrochemical cell was completed with a cylindrical Pt-mesh mounted around the reference electrode. The CTA of the samples (Figure 2) was determined to be 2 cm².

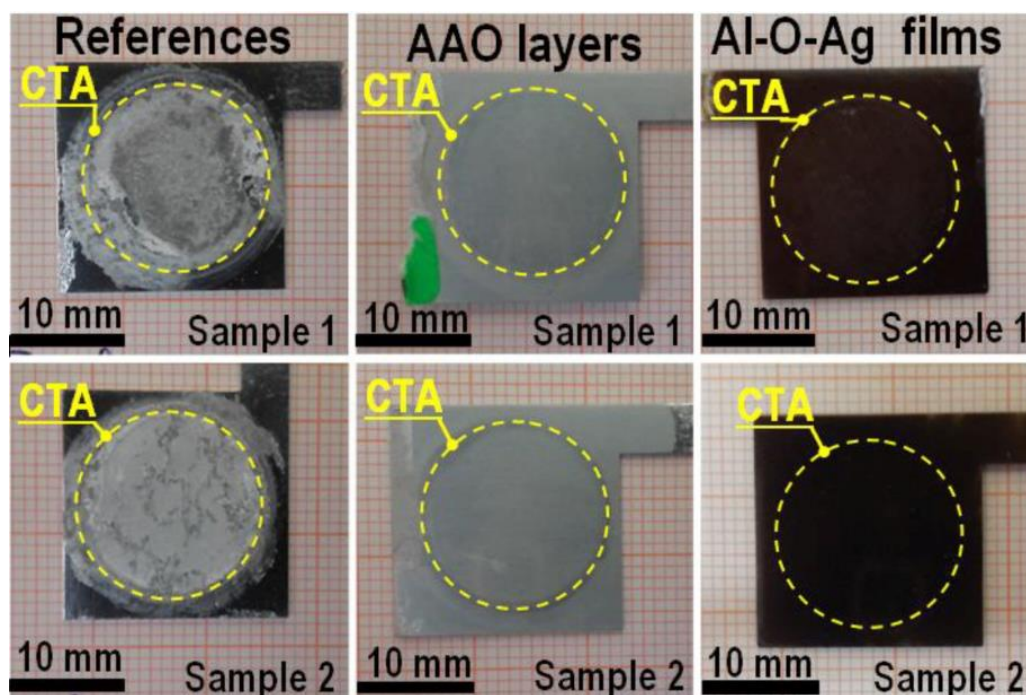


Figure 2. Images of investigated samples after extended periods of exposure to 3.5 % NaCl model corrosive medium

The EIS spectra were acquired in the frequency range from 10 kHz to 0.01 Hz, distributed in 50 measurement points with suitable amplitudes of the excitation signal against the *open circuit potential* (OCP), in order to acquire readable spectra. In this study, these amplitudes were 10 mV for the referent samples and 80 mV for the electrochemically treated ones, respectively. The application of different amplitudes was imposed by the need for overcoming the remarkable resistance of the AAO and Al-O-Ag layers, resulted from the dielectric properties inherent for the basic Al₂O₃ matrix. On the other hand, this amplitude value was too high for the reference samples, and causes polarization of the electrode, resulting in deformed impedance spectra and electrochemically enforced excessive corrosion.

The OCP values were determined directly prior to the respective EIS measurements. The subsequent potentiodynamic curves were acquired after the EIS spectra. The PDS were obtained from -30 to +500 mV against OCP with a voltage sweep rate of 5 mV s⁻¹. Since previous works [15,16], dedicated to anodization of technically pure AA1050 alloy, have shown that the electrochemical behavior of the samples reveals satisfying repeatability, the measurements were performed twice.

Results and discussion

X-ray diffractometry

The XRD spectra did not reveal any distinguishable features among the different samples. Only characteristic peaks for Al metallic substrates were registered for all types of samples. However, at low angles, between 10 and 30 angular degrees, a more intensive noise signal was registered for AAO and Al-O-Ag layers, which was clearer in the former case (Figure 3).

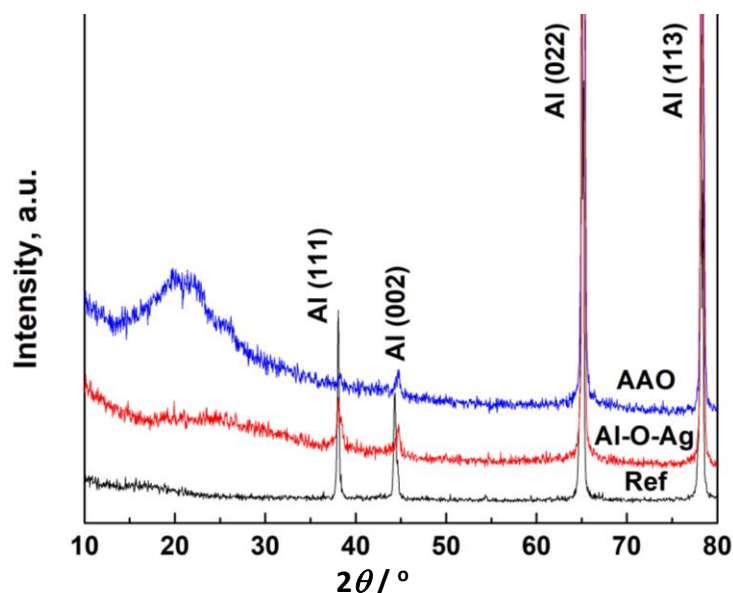


Figure 3. Superposition of XRD spectra acquired from samples of each investigated set

These features reveal that both AAO and Al-O-Ag layers possess definitely amorphous structures and no crystalline phase was formed. The flatter noisy plateau in the case of Al-O-Ag layer compared to the one of the AAO layer, is probably related to the shielding of AAO pore walls and bottoms by rather thin films of Ag deposits. This explication seems more plausible than any suggestion related to alterations of the thickness of the basic porous AAO matrix, promoted by the electrochemical Al-O-Ag layer formation. Indeed, previous research has shown that the thickness of formed AAO layer under such conditions is about 20 μm [61,62] and the AC-assisted silver deposition does not result in alteration of the oxide layer thickness [59,60]. Consequently, the lower XRD plateau in the case of Al-O-Ag is probably a result of the quenching of the X-ray signal, reflected by the porous AAO matrix.

The chemical composition of the Al-O-Ag system and oxidation states of its components were further investigated by means of XPS.

XPS analysis

In a previous study [60], we have not succeeded to detect any silver traces on the surface of the Al-O-Ag system, because Ag deposition proceeds on the pore bottoms and walls, the present sample was preliminary scraped by 1200 grid sandpaper prior to XPS analysis. This approach has enabled to

detect and analyze the silver deposits inside the pores of the oxide film. The XPS patterns acquired from the combined Al-O-Ag layer are shown in Figure 4.

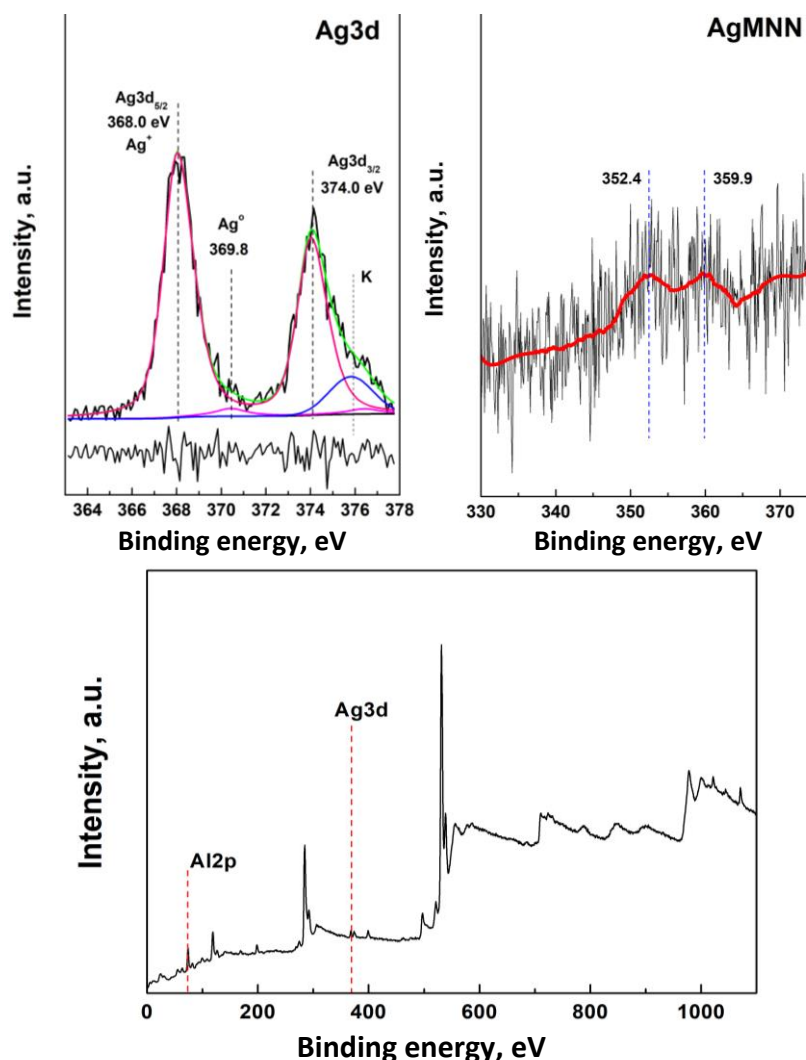
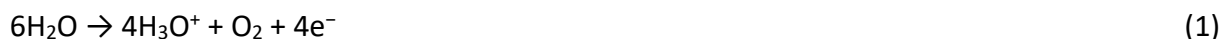


Figure 4. Integral and convoluted XPS spectra acquired from Al-O-Ag film

The detailed Ag3d spectrum possessed low intensity, being rather noisy due to the low content of this element inside the oxide layer (0.4 at%). The further deconvolution of this spectrum has revealed that this element is in the form of Ag^+ ions, since the main peak of $\text{Ag}3d_{5/2}$ is positioned at 368.0 eV, and the spin-orbital splitting is 6 eV, being typical for the ionic state of silver. Some negligible traces of metallic Ag^0 were detected, as well. The Auger spectrum of this element [63] also confirms the ionic state of this element. The spectrum noise has imposed further linear fitting. As a result, it was established that at both peaks associated with $\text{Ag } M_5N_{45}N_{45}$ and $\text{Ag } M_4N_{45}N_{45}$, the Auger electrons are situated at 352.4 eV and 359.9 eV, respectively. The values of the modified Auger electron parameters for these peaks are 720.4 and 727.9 eV, respectively. Consequently, silver deposition proceeds with oxidation of silver. Following the basic concepts [64-69], Ag oxidation probably proceeds with the inward O^{2-} ion migration from the electrolyte, across the surface of AAO pore bottoms and walls. This oxidation is a result of the applied potential during the negative semi-period of the AC-signal, during the electrochemical Ag-deposition (i.e. when the samples play the role of cathodes).

The positive semi-periods promote anodic polarizations, which in turn, result in oxygen evolution, providing oxygen enrichment near the electrode surface (Eq. 1).



These excessive amounts of dissolved oxygen near the Al-O-Ag layer oxidize the adjacent Ag^+ ions from the electrolyte (Eq. 2) and intensify the above-mentioned migration of O^{2-} ions, which react directly with Ag^+ ions, entered inside the pores.



Any amount of metallic Ag already deposited on AAO pores surfaces undergoes additional electrochemical (Eq. 3) and/or chemical (Eq. 4) oxidation:



Namely, the mahogany color of the obtained Al-O-Ag layers, shown in Figure 2, is the obvious evidence for the oxidized form of silver, proposed in previous studies [70].

The peak in the spectrum of the main metallic component Al, which composes Al-O-Ag layer is situated at 74.1 eV. This fact shows that aluminum is only in the form of Al_2O_3 (Eqs. 5 and 6). This oxide is predominantly formed during anodization, where the AAO layer grows in both inward and outward directions at the metal/oxide (Eq. 5) and oxide/electrolyte (Eq. 6) interface:



In conclusion, it can be inferred that the combined Al-O-Ag layer is composed by amorphous Al_2O_3 with Ag_2O deposits on the pore bottoms and walls. The oxidized state of silver deposits is evinced by the deconvoluted Ag 3d spectrum and the respective Auger spectra analyses.

The quantitative analysis of the element content of Al-O-Ag system has shown that the main elements composing the film are accompanied by alloying elements (*i.e.* Zn) and traces of the electrolytes used during the sample treatments (S, N, Cl, Cr and P), as shown in Table 2.

Table 2. Elemental composition of Al-O-Ag established by XPS analysis

Content, at%									
O	Ag	Al	Zn	S	N	Cl	Cr	P	Others
78.60	0.40	15.60	0.07	1.40	1.80	1.00	1.00	0.10	0.03

Table 2 also shows that although the layer is composed almost entirely of amorphous Al_2O_3 , the oxygen content is higher than the stoichiometric. This finding can be explained with entrapped water in the pores, which is retained by capillary forces. This is in accordance to previously published research [62], where it was established that anodization of this alloy results in definitely hydrophilic surface. The rather low silver content is a result of the low efficiency of the electrochemical silver deposition that was already established in another investigation [61], where the key reason for the low Ag deposition efficiency is ascribed to various electrochemical reactions which consume the applied electric charge.

Zn occurrence in Al-O-Ag layer is an obvious result of cationic currents passing from the metallic substrate to the growing oxide layer during anodization and also during the anodic semi-periods of the subsequent AC-polarization, as proposed by Charlesby [68]. This element was previously detected [62], and it was suggested that Zn content is a result of either Zn^{2+} ions migration from the metallic substrate to the growing oxide layer, or of direct inclusion of intermetallics during the inward growth of AAO at the metal/oxide interface.

The sulfur content originates from the sulfuric acid used for the sample anodization. The phenomenon of sulfur inclusion in AAO layers is described by Wernick *et al.* [71] and Thompson *et*

al. [72], and it was later confirmed at anodization of high doped [59,60] and low doped [61,62] aluminum alloys.

The rest detected elements originate from the solutions used for sample treatment and the formation of Al-O-Ag system. Thus, preliminary treatment supplies P and Cr from the brightening solution (containing H_3PO_4 and CrO_3) and probably from the basic alloy composition, Cl originates from the degreasing by CCl_4 , whereas N originates from $AgNO_3$ electrolyte used for silver deposition.

Electrochemical measurements

Because of the predominantly electrochemical inherence of the corrosion processes, the electrochemical analytical methods are most suitable for the determination of corrosion mitigation rate. Following the concepts described in previous studies [73], the corrosion protective properties can simply be divided into barrier ability and durability. The former can be described as rate of hindering of the access of corrosive species to the metallic surface, whereas the latter corresponds to the aptitude of the surface layer to keep its barrier properties after extended exposure to a corrosive medium. The results acquired *via* EIS and PDS after 24, 168 and 672 hours of exposure to 3.5 % NaCl model corrosive medium are discussed below.

EIS results

In order to obtain reliable results, the experiments were performed on two samples of each group. The impedance spectra acquired after 24 hours of exposure have shown quite different shapes (Figure 5), obviously requiring different *model equivalent circuits* (MEC) for numerical data acquisition.

The most remarkable difference between the reference and anodized samples is that the Nyquist plots of the former reveal semi-circles, whereas the latter are in form of slightly curved (for AAO) and straight (for Al-O-Ag) lines. Furthermore, after 168 hours of exposure, the reference samples show a slight increase of the semi-circle accompanied by disappearance of the low frequency tail. The comparison of impedance spectra in Figure 5 with the photographs in Figure 2 reveals that the reference samples have already corroded even before the initial 24 h period of exposure to the model corrosive medium. Indeed, the shapes of the spectra for these samples do not suffer considerable change, although the obvious impact of the corrosion on the sample surfaces shown in Fig. 2. The weak changes in the Nyquist plots are concordant with the negligible differences between the average diagrams in the respective Bode plots. Thus, for the referent samples, only a slight displacement of the phase shift maximum towards lower frequencies after 168 h of exposure is observed.

The obvious difference between the Nyquist plots for the referent and other groups of AAO and Al-O-Ag samples reveals that the formed oxide layers possess almost pure capacitive character, originated from the dense barrier layer under the pores. This capacitive behavior is even further enhanced after Ag deposition. On the other hand, the difference between AAO and Al-O-Ag layers is more evident in the respective Bode plots. The $(\log |Z| / \log f)$ curves of the referent samples reach 4.5, at 0.01 Hz, corresponding to the impedance magnitude $|Z|$ of $50 \text{ k}\Omega \text{ cm}^2$, while for both types of anodized specimens, this value is higher than $10 \text{ M}\Omega \text{ cm}^2$. This remarkable impedance value reveals the significant barrier properties possessed by both AAO and Al-O-Ag layers.

Although, both types of layers reveal typical capacitance spectra after 24 hours of exposure, AAO layers reveal a decay of phase shift $(\varphi / \log f)$ -curve at the high frequency domain after 672 hours of exposure. Consequently, the silver containing layers are more durable and keep their obvious barrier properties during the entire exposure period. Their distinct durability is a result of the deposition of silver oxide on the pore bottoms and walls. These notable differences in the shapes of the impedance spectra originate from the respective surface film properties and require different

MECs for the extraction of numerical data (Tables 3 and 4). All used MECs (Figure 6) are composed of consecutive RC unit connections.

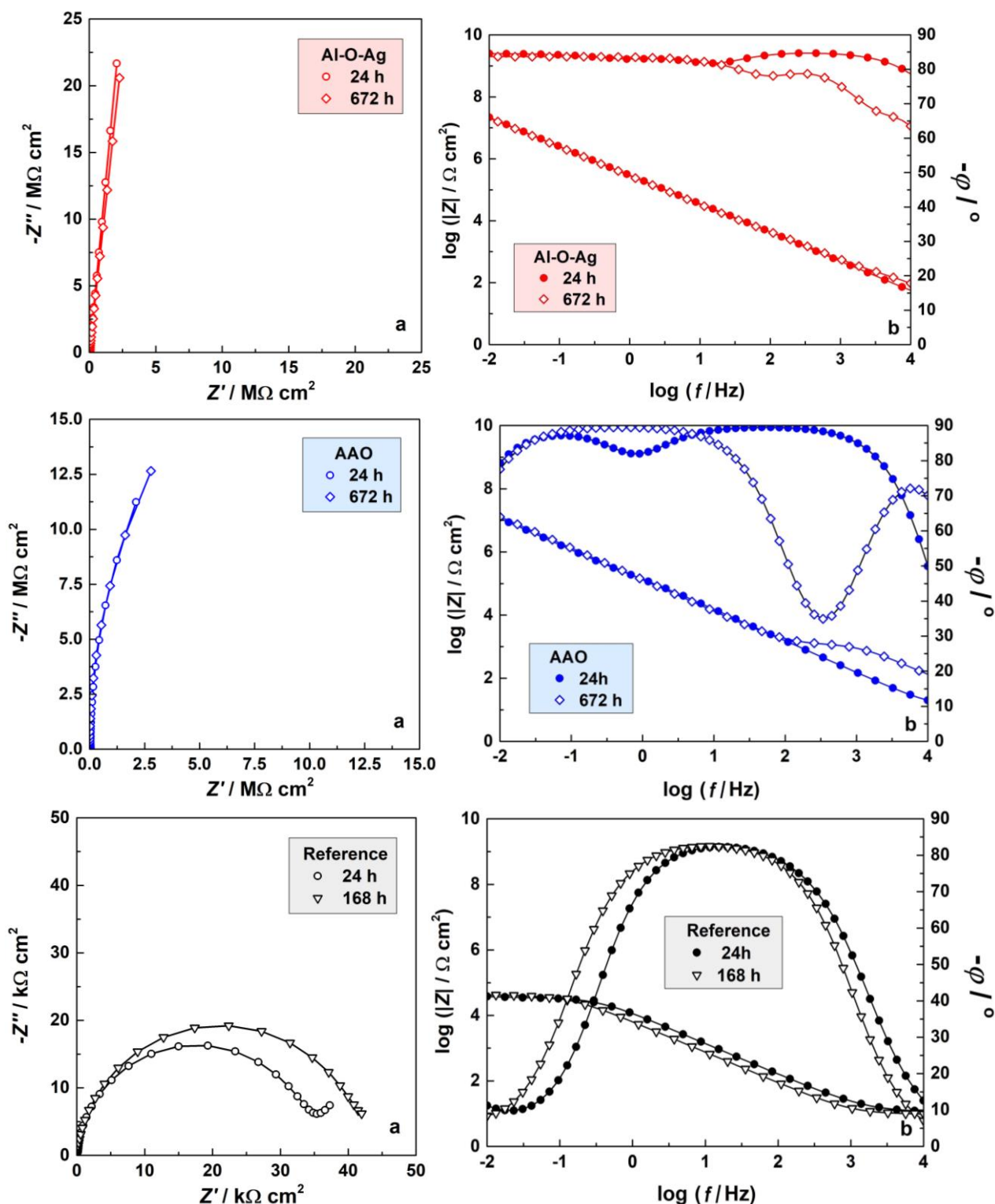


Figure 5. EIS spectra acquired after 24, 168 and 672 hours of exposure of the investigated samples to the model corrosive medium, represented in Nyquist (a) and Bode (b) plots

In some of MECs, the capacitances were replaced with constant phase elements (CPE) in the cases where the maxima of the phase shift ($\phi / \log f$)-curve does not reach -90° . This indicates an incomplete capacitance, revealing occurrence of defects in the surface oxide layer. In the present case, these oxide layer imperfections are related to its amorphous structure, which predetermines

variations in the density of the film. In both cases of AAO and Al-O-Ag layers, the oxide and electric double layers reveal pure capacitance, because the formed films possess remarkable thickness of about 20 μm, established in previous works [59,60,62]. In addition, according to the literature [11,12,64–66], these layers are composed of a thick porous layer and a dense barrier layer underneath. Namely, this dense layer predetermines the capacitive character of the whole AAO film. In the case of Al-O-Ag layers, a diffusion constant phase element (CPE_{diff}) is added which most probably is related to the hindering of the transport of interstitial ions and point defects through the dense barrier layer.

Thus, the appearance of this additional element reveals that the presence of silver obviously influences the characteristics of this underlayer. The influence of this process lies in the fact that it is performed in AC-regime.

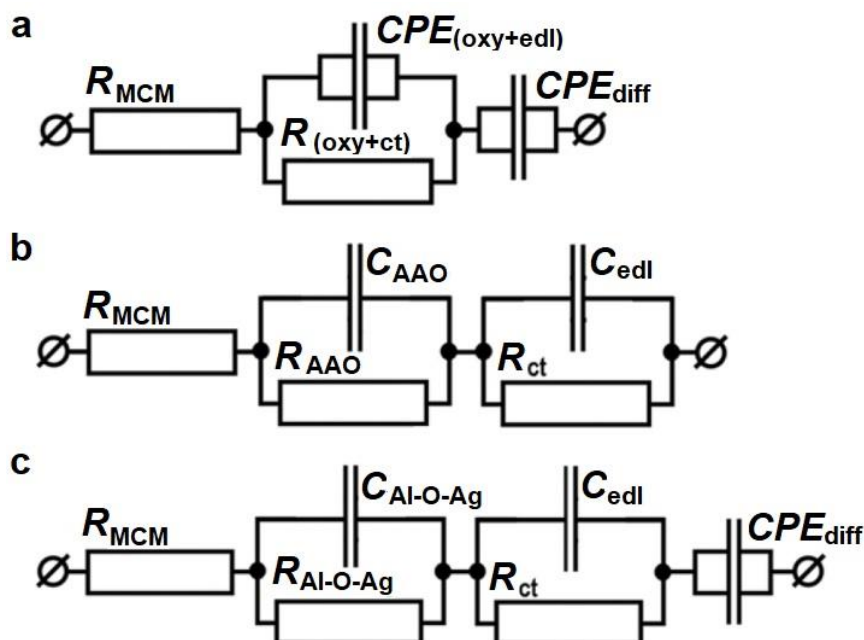


Figure 6. Model Equivalent Circuits used for the EIS spectra fitting for the (a) references, (b) AAO and (c) Al-O-Ag layers (R_{MCM} – resistance of the model corrosive medium; R_{oxy} – resistance of MCM penetrated inside the oxide layers, whose resistances are assigned as R_{AAO} and $R_{Al-O-Ag}$, respectively; R_{ct} – charge transfer reactions resistance, reflecting the electrochemical corrosion reactions under the oxide layer defects; $R_{(oxy+ct)}$ – resistance of the MCM penetrated through the oxide layer defects and of the charge transfer related to the electrochemical corrosion reactions between the penetrated MCM and the metallic surface domains under the oxide layer defects; $CPE_{(oxy+edl)}$ – constant phase element comprising the capacitance of the oxide layer and the electric double layer between the penetrated MCM and the bare metal surface under the defects. CPE_{diff} – constant phase element related to the obstruction of the diffusion of MCM components across the oxide layers defects (in the case of Al-O-Ag layer, the mentioned defects are under the pore bottoms); C_{AAO} and $C_{Al-O-Ag}$ – capacitances, originated from the insulating properties of the respective AAO and Al-O-Ag films; C_{edl} – capacitance of the electric double layer, between the bare metallic surface, under the defects and the MCM, penetrated across them)

Thus, the cathodic semi-periods cause partial cathodic dissolution, which results in localized alkalization, especially in the pores (Eq. 7). This reaction leads to a more defective dense underlayer, due to oxide dissolution (Eq. 8).



The polarization during the anodic semi-periods promotes oxidation processes, which result in a partial obstruction of the already formed defects in the dense sublayer. Thus, the free $\text{Al}(\text{OH})_4^-$ ions and the deposited Ag domains convert to insoluble oxides (Eqs. 9–11).



From recent works devoted to the electrochemical Ag_2O formation in alkaline electrolytes [74–77], it can be inferred that the localized alkalization inside AAO pores during the electrochemical silver deposition also contributes to the formation of Ag_2O .

The numerical data obtained by fitting of the acquired EIS spectra after 24 hours of exposure are summarized in Table 3.

Table 3. Numerical values of MEC elements acquired after fitting of EIS spectra obtained after 24 of exposure to MCM

Referent samples after 24 h of exposure			
Element	Sample 1	Sample 2	Average values
$R_{\text{MCM}} / \Omega \text{ cm}^2$	10.74 ± 0.09	11.29 ± 0.09	11.02 ± 0.09
$CPE_{\text{oxy+edl}} / \text{s}^n (\Omega \text{ cm}^2)^{-1}$	$(16.98 \pm 0.12) \times 10^{-6}$	$(11.91 \pm 0.11) \times 10^{-6}$	$(14.45 \pm 0.12) \times 10^{-6}$
n	0.97 ± 0.01	0.95 ± 0.01	0.96 ± 0.01
$R_{\text{oxy+ct}} / \Omega \text{ cm}^2$	$(26.38 \pm 0.83) \times 10^3$	$(40.40 \pm 1.06) \times 10^3$	$(33.39 \pm 0.95) \times 10^3$
$CPE_{\text{diff}} / \text{s}^n (\Omega \text{ cm}^2)^{-1}$	$(87.75 \pm 42.02) \times 10^{-5}$	$(70.25 \pm 31.97) \times 10^{-5}$	$(79.00 \pm 37.00) \times 10^{-5}$
n	0.63 ± 0.01	0.65 ± 0.01	0.64 ± 0.01
AAO-layers after 24 h of exposure			
$R_{\text{MCM}} / \Omega \text{ cm}^2$	12.61 ± 1.01	12.90 ± 1.22	12.76 ± 1.12
$C_{\text{AAO}} / \text{F cm}^{-2}$	$(1.33 \pm 0.03) \times 10^{-6}$	$(1.39 \pm 0.03) \times 10^{-6}$	$(1.39 \pm 0.03) \times 10^{-6}$
$R_{\text{AAO}} / \Omega \text{ cm}^2$	$(74.60 \pm 12.73) \times 10^6$	$(52.90 \pm 13.14) \times 10^6$	$(63.75 \pm 12.94) \times 10^6$
$C_{\text{edl}} / \text{F cm}^{-2}$	$(4.65 \pm 0.42) \times 10^{-6}$	$(4.26 \pm 0.41) \times 10^{-6}$	$(4.46 \pm 0.42) \times 10^{-6}$
$R_{\text{ct}} / \Omega \text{ cm}^2$	$(35.10 \pm 9.44) \times 10^3$	$(43.40 \pm 12.56) \times 10^3$	$(39.25 \pm 11.00) \times 10^3$
Al-O-Ag layers after 24 h of exposure			
$R_{\text{MCM}} / \Omega \text{ cm}^2$	9.58 ± 0.59	6.38 ± 0.37	7.98 ± 0.48
$C_{\text{Al-O-Ag}} / \text{F cm}^{-2}$	$(3.08 \pm 0.29) \times 10^{-6}$	$(4.58 \pm 0.33) \times 10^{-6}$	$(3.83 \pm 0.31) \times 10^{-6}$
$R_{\text{Al-O-Ag}} / \Omega \text{ cm}^2$	2189.40 ± 35.97	2263.00 ± 37.77	2226.00 ± 36.87
$C_{\text{edl}} / \text{F cm}^{-2}$	$(12.74 \pm 0.19) \times 10^{-6}$	$(10.47 \pm 1.39) \times 10^{-6}$	$(11.61 \pm 0.79) \times 10^{-6}$
$R_{\text{ct}} / \Omega \text{ cm}^2$	$(13.35 \pm 0.34) \times 10^3$	$(16.48 \pm 1.86) \times 10^3$	$(14.92 \pm 1.10) \times 10^3$
$CPE_{\text{diff}} / \text{s}^n (\Omega \text{ cm}^2)^{-1}$	$(60.75 \pm 0.18) \times 10^{-8}$	$(62.80 \pm 0.17) \times 10^{-8}$	$(61.78 \pm 0.18) \times 10^{-8}$
n	0.95 ± 0.01	0.93 ± 0.01	0.94 ± 0.01

The data of the capacitance elements (including CPEs) ascribed to the oxide films and the electric double layers are in the range of 1 to $17 \mu\text{F cm}^{-2}$ for all samples, revealing that the dense sublayers of both AAO and Al-O-Ag are with similar thicknesses to those of the native oxide layers of the referent samples. However, CPE_{diff} of Al-O-Ag layers are with three entire orders of magnitude lower than those of the referent samples. This fact shows that the diffusion of corrosive species from MCM (like Cl^- , OH^- ions, dissolved O_2 , etc.) through the Al-O-Ag layer is much more suppressed than this across the native oxide layers of the referent electrodes. The absence of CPE_{diff} in the case of AAO layers suggests that the barrier layer underneath the AAO pores is sparse, due to its amorphous structure. Indeed, the XRD analysis has revealed amorphous alumina, which has a density of between 2.66 and 3.40 g cm^{-3} .

[78,79], lower than this of the crystalline corundum. Hence, the barrier layer does not completely prevent the access of corrosive species like Cl⁻ ions towards the metallic surface.

Nevertheless, the average value of CPE_{diff} for Al-O-Ag layers is about 0.62 μF cm⁻² resembling great capacitive reactance. This fact is a result of the sealing of the pore bottoms and walls by Ag₂O, which strongly hinders the access of MCM ions to the metallic surface (across the dense AAO sublayer). However, due to the semiconductor properties of Ag₂O established by Talukdar *et al.* [80] the formed layer of silver oxide deposits also does not completely hinder the charge diffusion between the sealed pore bottoms and the metallic surface of the substrate. That is why, the exponential multiplier (n) of the CPE_{diff} element for Al-O-Ag systems does not reach unit, although it is close to this value.

At the end of the exposure periods (*i.e.* 168 h for the references and 672 h for the treated samples), the EIS spectra did not change in shape significantly (Figure 4). The numeric data acquired by fitting of EIS spectra at the end of the exposure periods are summarized in Table 4.

Table 4. Numerical values of MEC elements acquired after fitting of EIS spectra obtained at the end of the exposure to MCM

Referent samples after 168 h of exposure			
Element	Sample 1	Sample 2	Average values
$R_{MCM} / \Omega \text{ cm}^2$	8.12 ± 0.15	11.16 ± 0.06	9.64 ± 0.11
$CPE_{oxy+edl} / \text{s}^n (\Omega \text{ cm}^2)^{-1}$	(36.56 ± 0.62) × 10 ⁻⁶	(18.78 ± 0.18) × 10 ⁻⁶	(27.67 ± 0.40) × 10 ⁻⁶
n	0.90 ± 0.01	0.98 ± 0.02	0.94 ± 0.02
$R_{oxy+ct} / \Omega \text{ cm}^2$	(39.96 ± 0.27) × 10 ³	(42.80 ± 0.64) × 10 ³	(41.38 ± 0.46) × 10 ³
$CPE_{diff} / \text{s}^n (\Omega \text{ cm}^2)^{-1}$	(25.48 ± 1.55) × 10 ⁻⁴	(25.78 ± 1.52) × 10 ⁻⁴	(25.63 ± 1.54) × 10 ⁻⁴
n	0.73 ± 0.01	0.75 ± 0.01	0.74 ± 0.01
AAO layers after 672 h of exposure			
$R_{MCM} / \Omega \text{ cm}^2$	34.00 ± 3.55	23.00 ± 3.26	33.50 ± 3.44
$C_{AAO} / \text{F cm}^{-2}$	(1.18 ± 0.04) × 10 ⁻⁶	(1.22 ± 0.06) × 10 ⁻⁶	(1.20 ± 0.05) × 10 ⁻⁶
$R_{AAO} / \Omega \text{ cm}^2$	(63.30 ± 34.27) × 10 ⁶	(57.00 ± 27.91) × 10 ⁶	(60.20 ± 31.09) × 10 ⁶
$C_{edl} / \text{F cm}^{-2}$	(139.90 ± 26.57) × 10 ⁻⁹	(140.40 ± 21.66) × 10 ⁻⁹	(140.15 ± 24.12) × 10 ⁻⁹
$R_{ct} / \Omega \text{ cm}^2$	(1.15 ± 0.14) × 10 ³	(0.97 ± 0.12) × 10 ³	(1.06 ± 0.13) × 10 ³
Al-O-Ag layers after 672 h of exposure			
$R_{MCM} / \Omega \text{ cm}^2$	29.57 ± 0.35	22.71 ± 0.43	26.14 ± 0.39
$C_{Al-O-Ag} / \text{F cm}^{-2}$	(0.40 ± 0.02) × 10 ⁻⁶	(0.76 ± 0.04) × 10 ⁻⁶	(0.58 ± 0.03) × 10 ⁻⁶
$R_{Al-O-Ag} / \Omega \text{ cm}^2$	629.00 ± 1.11	637.30 ± 1.80	633.20 ± 1.46
$C_{edl} / \text{F cm}^{-2}$	(1.94 ± 0.10) × 10 ⁻⁶	(2.16 ± 0.16) × 10 ⁻⁶	(2.10 ± 0.16) × 10 ⁻⁶
$R_{ct} / \Omega \text{ cm}^2$	(9.50 ± 0.06) × 10 ³	(4.50 ± 0.05) × 10 ³	(7.00 ± 0.06) × 10 ³
$CPE_{diff} / \text{s}^n (\Omega \text{ cm}^2)^{-1}$	(63.45 ± 0.50) × 10 ⁻⁸	(63.19 ± 0.20) × 10 ⁻⁸	(63.32 ± 0.35) × 10 ⁻⁸
n	0.93 ± 0.01	0.93 ± 0.01	0.93 ± 0.01

The comparison of the EIS data from Tables 3 and 4 reveals that the samples did not suffer serious changes during their exposure to the 3.5 % NaCl solution. In the case of the referent samples, the lack of notable changes in the values of the impedance elements suggests that the corrosion process has begun even before the initial measurements after 24h of exposure. Thus, only CPE_{diff} has changed its value from 7.90 × 10⁻⁴ to 25.63 × 10⁻⁴ sⁿ (Ω cm²)⁻¹, revealing intensification of the perforation of the native oxide layer by Cl⁻ ions. However, the exponential multiplier (n) slightly increased its value, showing that after 168 hours of exposure, Cl⁻ ions penetration is already slightly

hindered by polyoxoaluminate corrosion products, as proposed elsewhere [73]. The values of all the rest capacitance and resistance elements of the reference electrodes remain almost the same, showing the steady corrosion of these samples in 3.5 % NaCl solution.

Even 672 hours of exposure did not change the impedance parameters of the obtained AAO and Al-O-Ag layers. In the case of AAO layers, only the charge transfer resistance (R_{ct}) has dropped from 39.25 k Ω cm² to 1.06 k Ω cm². Nevertheless, the electric double layer capacitance (C_{edl}) has changed from 4.46 to 0.14 μ F cm⁻², showing rise of the respective capacitive reactance most likely due to the obstruction of the defects in the dense sublayer by corrosion products. Furthermore, probably during the exposure of the anodized samples, Cl⁻ ions have reached the metallic surface, but the resulting corrosion products have already sealed the oxide layer, decreasing its electric capacity.

The weakest changes in the impedance parameters were registered for Al-O-Ag layers. The difference of all capacitance and resistance values was between two and four folds, and only the oxide layer parameters ($C_{Al-O-Ag}$ and $R_{Al-O-Ag}$) exceeded a half order of magnitude. The charge transfer resistance value detected after 672 hours of exposure was only twice lower than the initially registered one (from 14.92 to 7.00 k Ω cm²).

The explication for this fact is related to the sealing of the pore bottoms and walls by the Ag₂O deposits, which hinders the access of Cl⁻ ions to the substrate surface across the porous layer. Consequently, the corrosive species from MCM can reach the surface of the metallic substrate only through the oxide layer. Hence, these species would have to overcome about 20 μ m film thickness. The retention of the very low CPE_{diff} values of about 0.63 μ F cm⁻² and high, near to unit value of n for the entire 672 hours of exposure, confirm the suggestion for the considerable hindering of MCM ions reaching the metallic surface.

Potentiodynamic scanning (PDS) results

The images in Figure 7 reveal a great difference between the referent and the rest samples. This fact is an obvious consequence of the anodization process, which results in the growth of a thick alumina layer. In addition, the potentiodynamic curves show that the reference samples suffer intensive uniform corrosion, without any signs of localized corrosion. The absence of localized corrosion suggests that their surfaces are rather uniform, due to the relatively high purity of the basic substrate material (*i.e.* 99.5 % aluminum).

For comparison, the curves of both AAO and Al-O-Ag samples have almost horizontal anodic branches, showing almost complete passivation of the metallic substrates by the respective oxide layers. The deposition of Ag₂O did not show distinguishable contribution to the barrier ability of the resulting combined Al-O-Ag films, compared to the AAO ones, due to the low Ag-deposition efficiency, established in previous works [70]. Nevertheless, these films should be more durable than the anodized only layers, because of the pore bottoms and walls obstruction by the Ag₂O deposits, commented in the previous paragraph. In addition, the slight shifting of the corrosion potential (E_{corr}) values, and the relatively lower current densities of the curves acquired from Al-O-Ag films, compared to those of the AAO layers reveal the superior protective characteristics of the former ones. The Tafel slope analysis has uncovered additional information regarding the polarization resistance (R_p) and E_{corr} acquired from the potentiodynamic scanning curves.

The average values (AV) were determined with the deviations, predetermined by the difference between the higher (HV) and the lower (LV) modulus of R_p or E_{corr} values.

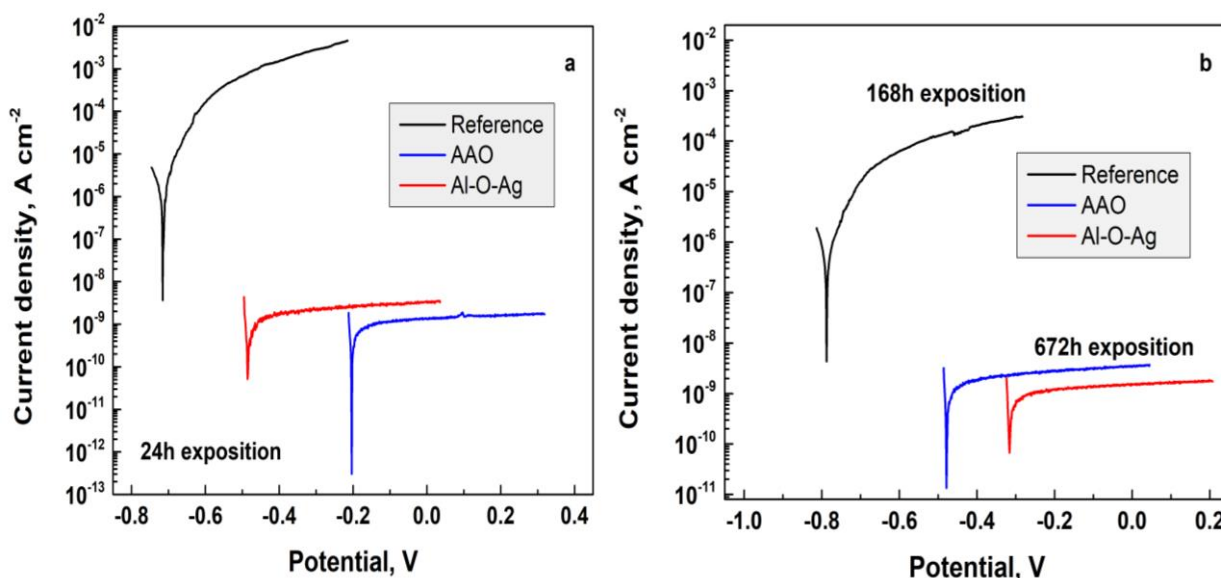


Figure 7. Potentiodynamic curves acquired after 24 hours (a) and at the end (b) of the exposure of investigated samples to MCM

$$AV = \frac{|HV| + |LV|}{2} \pm \frac{|HV| - |LV|}{2} \tag{12}$$

The numerical values, extracted from the Tafel slope analysis have also revealed that both AAO and Al-O-Ag layers render three orders of magnitude higher R_p values (in the order of 15 MΩ cm²), compared to those of the reference samples (about 10 kΩ cm²), as shown in Table 5.

Table 5. Numerical values of corrosion potential (E_{corr}) and polarization resistance (R_p), acquired from Tafel slope analysis of PDS curves obtained after 24 hours of exposure to MCM

Measure	Sample 1	Sample 2	Average values
Reference samples after 24 hours of exposure			
E_{corr} / mV vs. Ag/AgCl	-709	-715	-712 ± 3
R_p / kΩ cm ²	11.13	6.96	9.05 ± 2.09
AAO layers after 24 hours of exposure			
E_{corr} / mV vs. Ag/AgCl	-485	-381	-433 ± 52
R_p / kΩ cm ²	13.48×10 ³	17.88×10 ³	(15.68 ± 2.20)×10 ³
Al-O-Ag layers after 24 hours of exposure			
E_{corr} / mV vs. Ag/AgCl	-207	-226	-217 ± 10
R_p / kΩ cm ²	16.97×10 ³	14.13×10 ³	(15.55 ± 1.42)×10 ³

The anodization and silver deposition also result in remarkable shifting of E_{corr} in positive direction, from -712 mV for the references, to -217 mV for the Al-O-Ag layers. This E_{corr} shifting is an undoubted consequence of the modifications of the surface chemical composition, described in the previous paragraphs. The larger deviation between the AAO layers of ± 52 mV is probably due to the access of different MCM species (like Cl⁻, OH⁻ ions, dissolved O₂, etc.) through the pore bottoms to the surface of the metallic substrate. Such a distinguishable access registered for the AAO layers is a result of the amorphous structure of the investigated oxide films.

The final potentiodynamic scans acquired after 168 hours for the references and 672 hours of exposure for the rest groups have shown almost the same values (Table 6) like the initial ones (Table 5).

Table 6. Numerical values of corrosion potential (E_{corr}) and the polarization resistance (R_p), acquired after Tafel slope analysis of PDS curves obtained at the end of exposure to MCM

Measure	Sample 1	Sample 2	Average values
Reference samples after 168 hours of exposure			
E_{corr} / mV vs. Ag/AgCl	-755	-833	-794 ± 39
R_p / k Ω cm ²	11.41	8.70	10.05 ± 1.36
AAO layers after 672 hours of exposure			
E_{corr} /mV vs. Ag/AgCl	-291	-306	-299 ± 8
R_p /k Ω cm ²	15.63×10^3	15.94×10^3	$(15.79 \pm 0.15) \times 10^3$
Al-O-Ag layers after 672 hours of exposure			
E_{corr} /mV vs. Ag/AgCl	-253	-235	-244 ± 9
R_p /k Ω cm ²	16.51×10^3	14.09×10^3	$(15.30 \pm 1.21) \times 10^3$

This fact reveals that the samples did not suffer distinguishable changes during their exposure to MCM. In the case of the reference samples, it can be inferred that the corrosion process has begun even before the initial 24 hours of exposure. In the cases of AAO and Al-O-Ag films, the layers have kept their barrier ability, showing remarkable durability. The unique differences between the data in Tables 5 and 6 are related to the E_{corr} values of the AAO layers. After 672 hours of exposure, their values are displaced in a positive direction from about -433 mV to around -299 mV, probably due to obstruction of AAO layers by *Keggin*-like polyoxoaluminate corrosion products, as proposed in [73]. This suggestion also explains disappearance of the difference between E_{corr} values for AAO samples (from 52 to only 8 mV).

The comparison of Figure 7a and Figure 7b reveals that PDS curves of AAO and Al-O-Ag layers have exchanged their positions after 672 of exposure. This fact is confirmed by the data in Tables 5 and 6, as well. These data reveal that AAO layers have shifted their E_{corr} values with 134 mV in positive direction, whereas for Al-O-Ag layers the shift is by only -27 mV in the opposite direction. These facts show that Al-O-Ag system is more stable and does not change its chemical composition during the entire exposure period.

The considerable potential shift in the case of AAO towards nobler values is probably due to the already commented obstruction of AAO pores by polyoxoaluminate products. The difference between this potential shift for the respective oxide layers is an additional evidence for the remarkable durability of Al-O-Ag layer since its pore walls and bottoms are sealed by Ag₂O.

Conclusions

The present study is devoted to the structural and compositional characterization of AA1050 aluminum substrates after formation of thick oxide layers by means of anodization (AAO) and the subsequent electrochemical modification by silver deposition (Al-O-Ag). The used combination of analytical techniques XRD, XPS, and electrochemical tests after extended times of exposure to model corrosive medium, have led to several main conclusions. XRD patterns have shown completely amorphous structures of both AAO layer types, with and without silver.

XPS analysis of the chemical composition of Al-O-Ag layers has revealed that this film is composed of Al₂O₃ with traces of intermetallics originating from the metallic substrate and the used treatment solutions. Their content was even higher than this of silver. The most important conclusion from XPS analysis is that the deposited silver is in oxidized form. Furthermore, the determined oxygen content showed entrapped water in the layer pores.

The electrochemical measurements *via* EIS and PDS were performed after different periods of exposure to 3.5 % NaCl solution. This approach has enabled to determine the corrosion protective properties of the formed AAO and Al-O-Ag films. Thus, after 24 hours of exposure, both AAO and Al-O-Ag layers have revealed significant barrier ability against the access of the corrosive medium to the metallic substrates, compared to the reference samples. The impedance spectra, acquired from the formed films resembled this of ideal capacitor, demonstrating their apparent insulating properties.

The impedance spectra acquired after 672 hours of exposure were rather similar to those of the initial spectra (*i.e.* obtained after 24 hours). This fact showed that both types AAO and Al-O-Ag layers possess remarkable durability, keeping their barrier abilities after large times of exposure to the model corrosive medium.

The obviously different shapes of EIS spectra between the references and the treated samples were successfully fitted to different model equivalent circuits. The respective fitting procedures have enabled to acquire numerical data regarding all capacitances and resistances, composing the total impedances of the samples. The resulting data have shown that all impedance components keep their values for the entire exposure period. Besides, it was established that Ag₂O deposits on the pore bottoms and walls efficiently suppress the access of corrosive species to the substrate surface. Their presence enables supplemental extension of the oxide layer durability.

The PDS analyses have confirmed the inferences done for the EIS spectra. The polarization resistances of both AAO and Al-O-Ag layers had three orders of magnitude higher values, compared to those of the references. Besides, these values remained unchanged for the entire 672-hour period of exposure to the model corrosion medium.

Summarizing all the conclusions done for the respective analyses, it can be concluded that the electrochemically synthesized Al-O-Ag film on AA1050 alloy is composed mainly of amorphous Al₂O₃ with low silver content in form of Ag₂O deposits on AAO pore surface. Besides, the films possess distinguishable barrier ability and durability, determined under exposure to 3.5 % NaCl solution.

Acknowledgements: *The authors appreciate the financial support from the Bulgarian National Research Fund, via contract No: KΠ-06-H29/1.*

References

- [1] M. Lamberti, F. Escher, *Food Reviews International* **23** (2007) 407– 433.
- [2] O. Ayalon, Y. Avnimelech, M. Shechter, *Environmental Science and Policy* **3** (2000) 135–144.
- [3] C. C. Huang, H. W. Ma, *Science of the Total Environment* **324** (2004) 161– 172.
- [4] K. Marsh, B. Bugusu, *Journal of Food Science* **72** (2007) R39–R55.
- [5] S. P. Joshi, R. B. Toma, N. Medora, K. O'Connor *Food Chemistry* **83** (2003) 383–386.
- [6] M. Šeruga, J. Grgić, M. Mandić, *Zeitschrift für Lebensmittel-Untersuchung und Forschung* **198** (1994) 313–316.
- [7] F. Bianchi, M. Careri, M. Maffini, A. Mangia, C. Mucchino, *Rapid Communications in Mass Spectrometry* **17** (2003) 251–256.
- [8] A. Becaria, A. Campbell, S. C. Bondy, *Toxicology and Industrial Health* **18** (2002) 309–320.
- [9] J. Kandiah, C. Kies, *Biometals* **7** (1994) 57–60.
- [10] W. Stępniewski, J. M. Salerno, *Manufacturing Nanostructures*, W. Ahmed, N. Ali (Eds.) One Central Press, 2014, Chap. 12, p. 321.
- [11] K. Giffard, L. Arurault, C. Blanc, *Microporous and Mesoporous Materials* **235** (2016) 32– 41.
- [12] W. J. Stępniewski, *Current Nanoscience* **15(1)** (2018) 3–5.
- [13] K. Giffard, L. Arurault, C. Blanc, D. Di Caprio, *Surface and Interface Analysis* **51(12)** (2019) 1184–1193.
- [14] S. V. Kozhukharov, Ch. A. Girginov, *Phenomena and Theories in Corrosion Science, Methods of Prevention*, A. Gergely (Ed.), NOVA Sci. Publ. 2019, Chap. 1, p. 3.

- [15] Ch. A. Girginov, S. V. Kozhukharov, M. J. Milanes, *Bulgarian Chemical Communications* **50 A** (2018) 6–12.
- [16] S. V. Kozhukharov, Ch. A. Girginov, *Bulgarian Chemical Communications* **50-A** (2018) 13–21.
- [17] M. F. de Romero, S. Urdaneta, M. Barrientos, G. Romero, *CORROSION 2004 NACE International, Correlation between desulfovibrio sessile growth and OCP, hydrogen permeation, corrosion products and morphological attack on iron*, Houston, Ohio, 2004. Paper No. 04576.
- [18] J. R. Davis (Ed.), *Corrosion of aluminum and aluminum alloys*. ASM International, 1999, p. 152
- [19] R. Javaherdashti, *Phenomena and Theories in Corrosion Science, Methods of Prevention*, A. Gergely (Ed.) NOVA Sci. Publ. 2019. Chap. 7. p. 273.
- [20] V. S. Sinyavskii, V. D. Kalinin, *Protection of Metals* **41** (2005) 317–328.
- [21] N. Pornnumpa, M. Jariyaboon, *Engineering Journal* **23(4)** (2019) 171–181.
- [22] R. Rosliza, H. B. Senin, W. B. wan Nik, *Asean Journal on Science and Technology for Development* **25** (2008) 251–259.
- [23] P. M. Martin-Sanchez, A. A. Gorbushina, H. J. Kunte, J. Toepel, *Biofouling* **32** (2016) 635–644.
- [24] P. M. Martin-Sanchez, A. A. Gorbushina, J. Toepel, *International Biodeterioration and Biodegradation* **126** (2018) 216–223.
- [25] T. C. Dakal, A. Kumar, R. S. Majumdar, V. Yadav, *Frontiers in Microbiology* **7** (2016) Art. No. 1831.
- [26] A. B. Shatan, K. Vencílková, B. A. Zasońska, *Pharmaceutical Research* **36(10)** (2019) 1–12.
- [27] A. Mogrovejo-Valdivia, O. Rahmouni, N. Tabary, M. Maton, C. Neut, B. Martel, N. Blanchemain, *International Journal of Pharmaceutics* **556** (2019) 301–310.
- [28] S. Mozia, P. Sienkiewicz, K. Szymański, M. Zgrzebnicki, D. Darowna, A. Czyżewski, A. W. Morawski, *Journal of Chemical Technology and Biotechnology* **94(8)** (2019) 2497–251.
- [29] Y. Wang, Y. Wang, L. Su, Y. Luan, X. Du, X. Zhang, *Journal of Alloys and Compounds* **783** (2019) 136–140.
- [30] P. Sienkiewicz, D. Darowna, S. Mozia, *Machines. Technologies. Materials* **13(9)** (2019) 388–391.
- [31] M. Irfan, O. Polonskyi, A. Hinz, C. Mollea, F. Bosco, T. Strunskus, C. Balagna, S. Perero, F. Faupel, M. Ferraris, *Cellulose* **26(16)** (2019) 8877–8894.
- [32] V. A. Ponomarev, I. V. Sukhorukova, A. N. Sheveyko, E. S. Permyakova, A. M. Manakhov, S. G. Ignatov, N. A. Gloushankova, I. Y. Zhitnyak, O. I. Lebedev, J. Polčák, A. M. Kozmin, D. V. Shtansky, *ACS Applied Materials & Interfaces* **10(29)** (2018) 24406–24420.
- [33] G. Holla, R. Yeluri, A. K. Munshi, *Contemporary Clinical Dentistry* **3** (2012) 288–293.
- [34] L. Monyatsi, N. Mthombeni, M. Onyango, M. N. B. Momba, *International Journal of Environmental Research and Public Health* **9(1)** (2012) 244–271.
- [35] F. S. Arakawa, Q. L. Shimabuku-Biadola, S. de Lima Bazana, M. F. Silva, B. A. A. Filho, R. Bergamasco, *The Canadian Journal of Chemical Engineering* **97(9)** (2019) 2408–2418.
- [36] A. Rus, V–D. Leordean, P. Berce, *MATEC Web of Conferences*, **137** (2017). Art. No. 07007.
- [37] T. Ivanković, J. Dikić, S. Rolland du Roscoat, S. Dekić, J. Hrenović, M. Ganjto, *Water Science & Technology* **80(6)** (2019) 1085–1098.
- [38] M. T. Moustafa, *Water Science* **31(2)** (2017) 164–176.
- [39] A. Kędziora, M. Speruda, E. Krzyżewska, J. Rybka, A. Łukowiak, G. Bugła-Płoskońska, *International Journal of Molecular Sciences* **19(2)** (2018) 444–461.
- [40] C. Liao, Y. Li, S. C. Tjong, *International Journal of Molecular Sciences* **20(2)** (2019) 449–496.
- [41] K. Hea, M. Yana, Z. Huang, G. Zeng, A. Chen, T. Huang, M. Peng, G. Chen, *Applied Clay Science* **171** (2019) 38–47.
- [42] I. Shah, R. Adnan, W. Saime, W. Nga, *International Journal of Chemistry* **135** (2014) 1459–1471.
- [43] V. V. Torbina, A. A. Vodyankin, S. Ten, G. V. Mamontov, M. A. Salaev, V. I. Sobolev, O. V. Vodyankina, *Catalysts* **8** (2018) Art. No. 447.
- [44] M. L. Zou, M. L. Du, H. Zhu, C. S. Xu, Y. Q. Fu, *Journal of Physics D: Applied Physics* **45** (2012) 1–7.
- [45] J. Y. Park, K. J. Hwang, J. W. Lee, I. H. Lee, *Journal of Materials Science* **46** (2011) 7240–7246.
- [46] M. Padervand, H. Salari, S. Ahmadvand, M. R. Gholami, *Research on Chemical Intermediates* **38** (2012) 1975–1985.
- [47] R. Senthil, A. Khan, J. Pan, S. Osman, V. Yang, T. R. Kumar, Y. Sun, X. Liu, *Colloids and Surfaces A* **586** (2020) Art. No. 124183.
- [48] H-T. Ren, Y. Liang, X. Han, Y. Liu, S-H. Wu, H. Bai, S-Y. Jia, *Applied Surface Science* **504** (2020) Art. No. 144433.

- [49] U. H. Bhatti, D. Sivanesan, S. Nam, S. Y. Park, H. Baek, *ACS Sustainable Chemistry & Engineering* **7(12)** (2019) 10234–10240.
- [50] H. Wang, B. Li, J. Mei, C. Gao, Z. Li, S. Xu, *Fullerenes, Nanotubes and Carbon Nanostructures* **27(5)** (2019) 410–416.
- [51] J. Hu, H. Xu, S. Wang, W. Jia, Y. Cao, *Separation and Purification Technology* **226** (2019) 95–108.
- [52] W. Panpa, S. Jinawath, D. P. Kashima, *Journal of Materials Research and Technology* **8(6)** (2019) 5180–5193.
- [53] N. K. Nasab, Z. Sabouri, S. Ghazal, M. Darroudi, *Journal of Molecular Structure* **1203** (2020) Art. No. 127411.
- [54] T. Liu, X. Zhang, F. Zhao, Y. Wang, *Applied Catalysis B: Environmental* **251** (2019) 220–228.
- [55] Y. Li, Q. Wang, H. Wang, J. Tian, H. Cui, *Journal of Colloid and Interface Science* **537** (2019) 206–214.
- [56] A. Cai, Y. Sun, L. Du, X. Wang, *Journal of Alloys and Compounds* **644** (2015) 334–340.
- [57] M. E. Assal, M. R. Shaik, M. Kuniyil, M. Khan, A. Al-Warthan, A. Ibrahim, A. Ravi, V. Mohammed, R. H. Siddiqui, S. F. Adi, *Arabian Journal of Chemistry* **12** (2019) 54–68.
- [58] E. Bu, Y. Chen, C. Wang, Z. Cheng, X. Luo, R. Shu, J. Zhang, M. Liao, Z. Jiang, Q. Song, *Chemical Engineering Journal* **370** (2019) 646–657.
- [59] Ch. Girginov, S. Kozhukharov, D. Kiradzhyska, R. Mancheva, *Electrochimica Acta* **292** (2018) 614–627.
- [60] S. Kozhukharov, Ch. Girginov, A. Tsanev, M. Petrova, *Journal of the Electrochemical Society* **166(10)** (2019) C231–C242.
- [61] Ch. Girginov, S. Kozhukharov, M. Milanec, M. Machkova, *Materials Chemistry and Physics* **198(1)** (2017) 137–144.
- [62] S. Kozhukharov, Ch. Girginov, I. Avramova, M. Machkova, *Materials Chemistry and Physics* **180** (2016) 301–313.
- [63] A. M. Ferraria, A. P. Carapeto, A. M. Botelho do Rego, *Vacuum* **86** (2012) 1988–1991.
- [64] G. D. Sulka, *Nanostructured Materials in Electrochemistry*, A. Eftekhari (Ed.), Wiley-VCH Verlag, 2008, Chap. 1, pp. 1-116.
- [65] G. E. Thompson, Y. Xu, P. Skeldon, K. Shimizu, S. H. Han, G. C. Wood, *Philosophical Magazine B* **55** (1987) 651–667.
- [66] G. E. Thompson, *Thin Solid Films* **297** (1997) 192–201.
- [67] A. Girginov, M. Bojinov, *Journal of the University of Chemical Technology and Metallurgy* **43** (2008) 29–36.
- [68] A. Charlesby, *Proceedings of the Physical Society. Section B* **66** (1953) 317–329.
- [69] L. Andreeva, S. Ikonopisov, *Electrochimica Acta* **6** (1970) 1070–1074.
- [70] D. Kiradzhyska, R. Mantcheva, Ch. Girginov, S. Kozhukharov, *Journal of Chemical Technology and Metallurgy* **53(4)** (2018) 745–748.
- [71] S. Wernick, R. Pinner, P. Sheasby, *ASM International* **5** (1987) 289–368.
- [72] G. E. Thompson, G. C. Wood, *Treatise on Materials Science and Technology*, J. C. Scully (Ed.), Acad. Press, New York, 1983, p. 205.
- [73] S. Kozhukharov, V. Kozhukharov, M. Wittmar, M. Schem, M. Aslan, H. Caparrotti, M. Veith, *Progress in Organic Coatings* **71(2)** (2011) 198–205.
- [74] B. M. Jović, V. D. Jović, *Journal of the Serbian Chemical Society* **69(2)** (2004) 153–166.
- [75] J. Ambrose, R. G. Barradas, *Electrochimica Acta* **19(11)** (1974) 781–786.
- [76] T. U. Hura, W. S. Chun, *Journal of the Electrochemical Society* **152** (2005) A179–A185.
- [77] S. S. A. El Rehim, H. H. Hassan, M. A. M. Ibrahim, M. A. Amin, *Monatshefte für Chemie* **129** (1998) 1103–1117.
- [78] C. Shi, O. L. G. Alderman, D. Berman, J. Du, J. Neuefeind, A. Tamalonis, J. K. Richard Weber, J. You, C. J. Benmore, *Frontiers in Materials* **6** (2019) Art. No. 38, 1–15.
- [79] S. P. Adiga, P. Zapol, L. A. Curtis, *Physical Review B* **74** (2006) Art. No. 064204, 1–8.
- [80] M. I. Talukdar, E. H. Baker, *Solid State Communications* **7(2)** (1969) 309–310.